

KINETIC INVESTIGATION ON PARTIALLY OXIDIZED HUADIAN OIL SHALE BY THERMOGRAVIMETRIC ANALYSIS

FENGTIAN BAI^(a), YOUHONG SUN^{(a)*}, YUMIN LIU^(a),
BAOCHANG LIU^(a), MINGYI GUO^{(a)*}, XIAOSHU LÜ^(a,b),
WEI GUO^(a), QIANG LI^(a), CHUANBIN HOU^(a),
QIUWEN WANG^(a)

^(a) College of Construction Engineering, Jilin University, Changchun 130021, P.R. China

^(b) Department of Civil and Structural Engineering, School of Engineering, Aalto University, P.O. Box 12100, Espoo, Finland

Abstract. *The kinetic parameters of Huadian oil shale and its solid residues after preheating treatment at different temperatures were evaluated by thermogravimetric (TG) analysis. As per distinct properties of oil shale, TG curves were divided into five separate stages during pyrolysis. The kinetic parameters were calculated based on TG results related to three stages ranging from 250 to 550 °C, using the Arrhenius theory and Coats-Redfern and Flynn-Wall-Ozawa methods. The results showed that the burning of oil shale and its solid residues was a complicated multi-step kinetic process. The activation energies of residues were reduced after preheating treatment below 300 °C. Moreover, the activation energies calculated from the Coats-Redfern method increased with increasing heating rate.*

Keywords: *oil shale, thermogravimetric analysis, kinetic analysis, activation energy.*

1. Introduction

The past two decades have witnessed a tremendous growth of global energy demand. This has significantly encouraged the exploitation of promising alternative resources – shale oil and gas, which have attracted more and more attention due to huge reserves and great commercial potential.

Generally, retorting processes for oil shale can be divided into two types: ex situ (aboveground) technologies, such as the Kiviter process employed in

* Corresponding author: e-mail syh@jlu.edu.cn; guomingyi@jlu.edu.cn

Estonia, the Tosco II technology used in the USA and the Fushun-type retorting applied in China [1], and in situ methods, such as ICP of Shell, ElectrofracTM by ExxonMobil, USA, and Chevron's technology, USA [2]. However, the oil shale industry employing these technologies [3] has yet to tackle with several critical problems, such as harmful semicoke waste, complicated multistage technological scheme for retorting [4], high energy consumption in ICP, etc. Recently, the oil shale self-heating retorting [5] and topochemical reaction [6] have been introduced as low-energy oil shale conversion methods. A specific feature of these methods is that oil shale is preheated in the presence of air. In the self-heating retorting process, oil shale is first preheated from room temperature to 300 °C under N₂, then at 150 °C in the presence of air, which triggers the self-heating effect. In case of the topochemical reaction, a chemical reaction between oil shale and oxygen takes place. However, up to now, no research on the kinetic analysis of the shale residues after partial oxidation treatment has yet been made.

Thermogravimetry (TG) has been widely used to analyze devolatilization characteristics, the effect of temperature on thermal degradation, and kinetic parameters of oil shale [6–10]. TG analysis can be performed using both isothermal and non-isothermal methods, while the non-isothermal analysis has gained in popularity to study the kinetic behaviour of oil shale. Kök [11–17] has investigated the effect of heating rate and clay content on the kinetics of the fossil fuel combustion and pyrolysis by using TG and different kinetic models. Jiang et al. [18] have reported the mechanism and mathematical model of Huadian (HD) oil shale pyrolysis with different oil shale particle sizes and different heating rates. Yan et al. [19] have studied the interaction between oil shale and shale char during the co-pyrolysis. Nevertheless, researches on the activation energy of solid residues after partial oxidation treatment have been rare [20].

In this work, the thermal behaviour and kinetic mechanism of raw and partially oxidized Huadian oil shale were investigated. The non-isothermal TG analysis and Coats-Redfern (C-R) and Flynn-Wall-Ozawa (FWO) methods were used to determine the kinetic parameters of oil shale at temperatures ranging from 250 to 550 °C. It was noted that the activation energy of partially oxidized oil shale (below 300 °C) was decreased. It is expected that this study not only inspires research on the mechanism of new methods of oil shale processing, such as self-heating retorting [5] and topochemical reaction [6], but also introduces new ideas into oil shale industry.

2. Experimental section

2.1. Materials

The oil shale used was obtained from the Gonglangtou mine located in Huadian (HD), China, and was received as hard, dark gray blocks with no particular smell. The physical properties of oil shale are summarized in

Table 1. The ash analysis was performed using a Philips PW 1404/10 XRF spectrometer, the results are presented in Table 2.

Table 1. Physical properties of HD oil shale

Proximate analysis, ad		Ultimate analysis, wt%, ad		Fischer assay analysis, wt%, ad		Density, kg m ⁻³
Volatiles, wt%	40.02	C	34.49	Shale oil	14.08	1570
Fixed carbon, wt%	6.34	H	4.227	Gas	8.43	
Ash, wt%	50.29	N	0.9	Water	4.84	
Moisture, wt%	3.35	S	1.589	Residue	72.65	
Calorific value, kJ kg ⁻¹	14724					

Table 2. Ash content of HD oil shale, mass%

SiO ₂	Al ₂ O ₃	Fe ₂ O ₃	CaO	MgO	K ₂ O	Na ₂ O	TiO ₂	P ₂ O ₅	MnO
63.52	16.49	9.65	4.43	2.07	1.74	0.89	0.74	0.27	0.20

The partially oxidized oil shale was obtained by the preheating treatment from 100 °C to 600 °C in a tube furnace, which was electrically heated and air-swept at a continuous flow rate of 10 mL min⁻¹ at STP. Then a reaction between oil shale and oxygen, known as the partial oxidation of kerogen, followed [6]. The procedure was carried out in three steps. First, block oil shale samples (2 × 2 × 6 cm³, 35–40 g) were placed in the center of the quartz tube and heated at a rate of 5 °C min⁻¹ to a specific temperature. Once the desired temperature was achieved, the samples were then held for 100 min to ensure that their masses remain constant. Thereafter the reactor cooled down to room temperature and the solid residues were collected.

For convenience the samples were labeled S_{raw}, S₁₀₀, S₂₀₀, S₃₀₀, S₄₀₀, S₅₀₀, S₆₀₀, where subscripts represent raw oil shale or preheating treatment temperatures. For example, S₁₀₀ denotes the solid residue collected after preheating treatment at 100 °C.

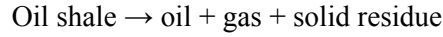
2.2. Apparatus and experimental procedures

TGA and differential thermal analyses (DTA) were performed using a Netzsch STA 449C thermal analyzer system (Germany) under air atmosphere (50 mL min⁻¹). The X-ray diffraction (XRD) pattern was performed using a Rigaku D/MAX 2550 diffractometer (Japan) with Cu K α radiation at 50 kV and 200 mA. The Fourier transform infrared (FTIR) spectrum (KBr) was obtained using a Bruker IFS 66V/S FTIR spectrometer (Germany) in the mid-IR region of 400–4000 cm⁻¹.

Before conducting the above analytical tests, the prepared samples were finely ground (< 63 μ m) and prepared according to ASTM standards. Duplicate experiments were performed to ensure reproducibility.

2.3. Kinetic modeling

Modeling of a reaction for the combustion and pyrolysis processes of natural matter is extremely complicated, because in these processes several components are oxidized simultaneously. The organic matter, or kerogen, present in oil shale is a solid substance insoluble in water. The thermal decomposition of oil shale in a non-isothermal mode could be represented by the following reaction:



The rate of the kinetic process is usually expressed by the following equation:

$$\begin{cases} \frac{dx}{dt} = kf(x) \\ f(x) = (1-x)^n \end{cases}, \quad (1)$$

where $f(x)$ is a dependent kinetic model function, x is the extent of conversion, t is the time, k is the rate constant and n is the order of reaction. The extent of conversion can be defined as follows:

$$x = \frac{m_0 - m}{m_0 - m_f}, \quad (2)$$

where m is the weight of the sample at time t , m_0 and m_f refer to the initial and final weights of the sample. According to the Arrhenius equation, the temperature dependence of the rate constant is:

$$k = A \exp\left(-\frac{E}{RT}\right), \quad (3)$$

where A is the pre-exponent factor, E is the activation energy, T is the absolute temperature and R is the universal gas constant. For non-isothermal conditions, the constant heating rate β presents a linear relation between time and temperature:

$$\beta = \frac{dT}{dt}. \quad (4)$$

Substituting Equations (3) and (4) in Equation (1) gives:

$$\frac{dx}{dT} = \frac{A}{\beta} \exp\left(-\frac{E}{RT}\right) f(x). \quad (5)$$

The above equation can be used to determine E and A by employing TG data. Approaches, such as direct Arrhenius, C-R [21], Horowitz-Metzger, Kissinger and FWO methods [22–24], can be applied to determining kinetic parameters. The direct Arrhenius, Horowitz-Metzger and C-R methods

employ data obtained only at one heating rate, while the single scanning, Kissinger and FWO methods are based on measurements made at different heating rates (isoconversional method). The attraction of the isoconversional method derives mainly from its ability to afford activation energy values without the necessity for presuming the analytical form of the conversion model [25]. In the present work, kinetic analysis was performed using C-R and FWO methods.

2.3.1. C-R method

The C-R method is widely used for the calculation of kinetic parameters. In order to simplify calculations, the order of reaction (n) is assumed unity. After performing a series of mathematical transformations, the final form of the first order C-R equation is as follows:

$$\ln \left[-\frac{\ln(1-x)}{T^2} \right] = \ln \frac{AR}{\beta E} - \frac{E}{R} \cdot \frac{1}{T}. \quad (6)$$

Plotting the left-hand side of Equation (6) against $1/T$ gives a straight line having a slope of $-E/R$ and an intercept of $\ln(AR/\beta E)$. Using TG data, the activation energy E and the pre-exponential factor A can be calculated.

2.3.2. FWO method

The FWO method is based on an assumption that the rate of a conversion reaction is only a function of temperature, and that the reaction model is not dependent on temperature or heating rate [26, 27]. This method is based on the following equation:

$$\log \beta = \log \frac{AE}{Rg(x)} - 2.315 - 0.4567 \frac{E}{R} \cdot \frac{1}{T}, \quad (7)$$

where $g(x)$ is the integral form of the reaction model.

Thus, for $x = \text{const}$, the plot of $\log \beta$ vs $1/T$ constructed from TG data obtained at different heating rates should be a straight line whose slope allows evaluation of the activation energy.

3. Results and discussion

3.1. Characterization of raw Huadian oil shale

Various functional groups were observable in the FTIR spectrum of raw HD oil shale (Fig. 1a). The spectrum consists of stretching and bending vibrations from the aliphatic and aromatic groups of kerogen, which overlap with the peaks of minerals such as carbonates, quartz, and clay. A sharp band at 3700 cm^{-1} is attributable to kaolinite; a sharp band at 3620 cm^{-1} results from

montmorillonite in the shale [28]. The aliphatic hydrocarbon stretching bands observed at 2920 cm^{-1} ($\nu_{\text{as}}\text{ CH}_2$) and 2850 cm^{-1} ($\nu_{\text{s}}\text{ CH}_2$) and the aromatic bands at 1620 and 736 cm^{-1} provide further evidence that a significant amount of organic compounds is present in the HD oil shale [29, 30]. These data illustrate that the kerogen of HD oil shale is aliphatic in nature and has been derived from immature lacustrine sediments [8, 31–33]. The characteristic peaks of calcite are at 1800 , 1420 and 872 cm^{-1} . The three unresolved bands at 1164 , 1105 and 420 cm^{-1} are due to pyrite in oil shale [9, 28]. The bands at 800 and 778 cm^{-1} are characteristic peaks of quartz.

The XRD patterns (Fig. 1b) of raw oil shale provided further evidence in support of FTIR results, especially those for inorganic minerals. As seen from Figure 1b, quartz is clearly the dominant phase in the minerals of HD oil shale. In addition to pyrite and feldspars, carbonate minerals and clays are also present in different proportions. However, the mineral crystallization of HD oil shale is generally poor. Moreover, the variable pattern between 5° and 29° reveals that organic matter is mostly amorphous [29].

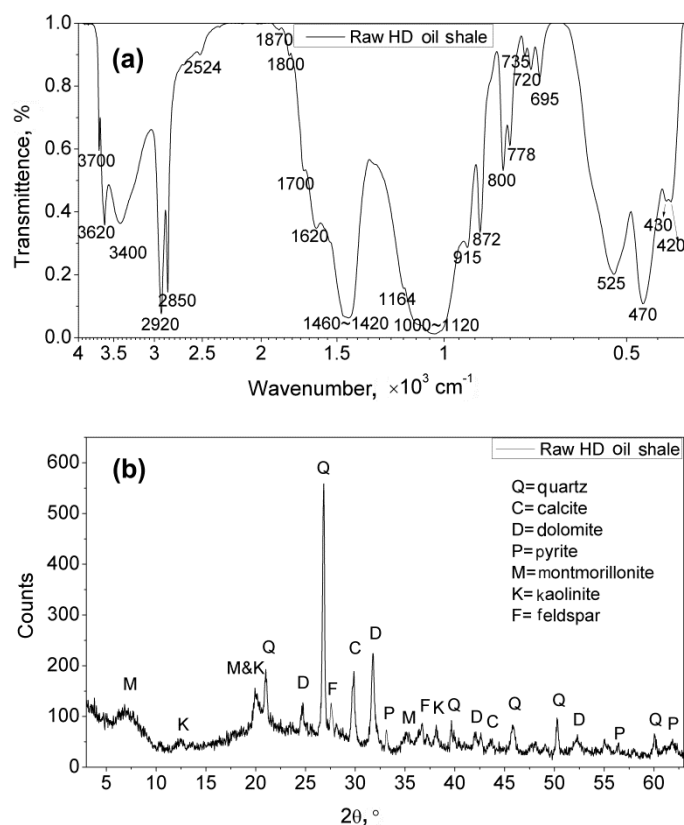


Fig. 1. (a) FTIR and (b) XRD spectra of raw HD oil shale samples.

3.2. TG, DTA and DTG of raw Huadian oil shale

Figure 2 shows the TG, DTA and DTG curves for raw HD oil shale in an air atmosphere at a heating rate of $10\text{ }^{\circ}\text{C min}^{-1}$. The experiments were repeated several times and showed good reproducibility. The stages were as follows:

(a) Below $200\text{ }^{\circ}\text{C}$, the mass loss can be mainly attributed to evaporation of water, especially adsorbed and interlayer water from clay minerals.

(b) In a temperature range from $250\text{ }^{\circ}\text{C}$ to $550\text{ }^{\circ}\text{C}$, a significant mass loss and three main exothermic reactions took place. This stage mainly involves the decomposition of bitumen and kerogen into volatiles. The entire process is exothermic and the reaction rapid.

(c) Above $600\text{ }^{\circ}\text{C}$, the final mass loss was observed. This stage is governed by the thermal decomposition of carbonates and clay minerals. The reaction is strongly endothermic under air atmosphere.

The entire reaction process for oil shale can be divided into five stages [6, 7, 11, 12]: (a) distillation, (b) low-temperature oxidation (LTO), (c) moderate-temperature oxidation (MTO), (d) high-temperature oxidation (HTO), and (e) decomposition of organic residues and inorganic minerals. LTO, MTO and THO are mostly dominated by the pyrolysis of organic matter. This study mainly focuses on the dynamic characteristics of organic matter decomposition at different preheating temperatures. The kinetic study of stages (a) and (e) was not undertaken.

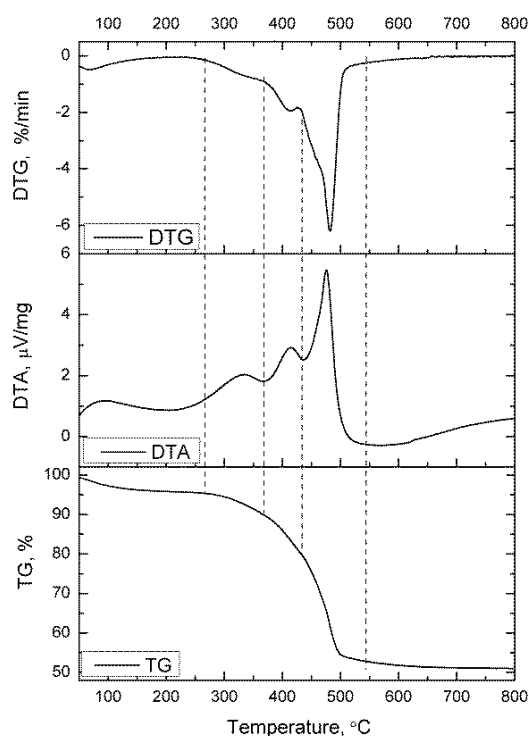


Fig. 2. TG, DTA and DTG curves of raw HD oil shale samples in an air atmosphere.

3.3. Analysis of kinetic characteristics by the C-R method

3.3.1. Kinetics of raw Huadian oil shale and solid residues at a heating rate of $10\text{ }^{\circ}\text{C min}^{-1}$

From the DTG curves shown in Figure 3, three stages of organic matter pyrolysis at $10\text{ }^{\circ}\text{C min}^{-1}$ can be clearly observed in S_{100} , which is similar to S_{raw} ; the rates of mass loss of S_{raw} and S_{100} increase from LTO to HTO. For S_{200} and S_{300} , the rate of pyrolysis in MTO is the highest, decreasing in HTO. As the preheating temperature increases, thermal reactions of oil shale take place, the LTO and HTO stages disappear and the rate of pyrolysis of S_{400} , S_{500} and S_{600} in MTO declines. Moreover, the peak temperature of S_{400} , S_{500} and S_{600} increases and the DTG peaks shift to higher temperature. This is because after high-temperature pretreatment less kerogen is left, and DTG peaks of the residue shift to the high-temperature region. The characteristic temperatures of and the mass loss values of oil shale samples in each thermal degradation stage are listed in Table 3. For S_{raw} , S_{100} , S_{200} and S_{300} , the mass loss in LTO and MTO stages increases successively, accompanied by a decrease in the HTO stage, indicating that the reactions occurred in the

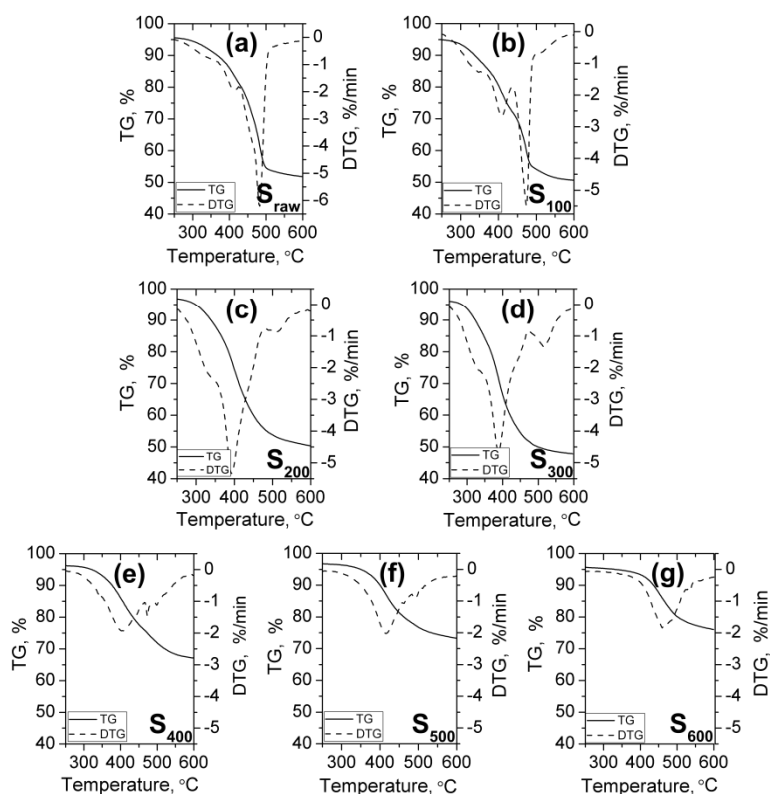


Fig. 3. TG and DTG curves of HD oil shale samples at a heating rate of $10\text{ }^{\circ}\text{C min}^{-1}$.

Table 3. Reaction intervals, peak temperatures and mass losses of HD oil shale samples at a heating rate of 10 °C min⁻¹

Sample label	LTO			MTO			HTO			TML ^d , %
	RI ^a , °C	PT ^b , °C	ML ^c , %	RI, °C	PT, °C	ML, %	RI, °C	PT, °C	ML, %	
S _{raw}	280–370	332	4.86	370–442	405	11.96	442–502	474	23.40	40.22
S ₁₀₀	290–375	340	8.47	375–437	408	13.09	437–492	471	17.37	38.92
S ₂₀₀	280–362	335	12.71	362–479	390	26.56	479–540	510	7.62	46.89
S ₃₀₀	280–439	330	36.05	439–482	388	7.11	482–539	516	6.19	49.35
S ₄₀₀				320–464	407	19.03	465–551	481	7.79	26.82
S ₅₀₀				336–545	408	20.60				20.60
S ₆₀₀				410–554	457	14.20				14.20

^a Reaction interval^b Peak temperature^c Mass loss^d Total mass loss, including LTO, MTO and HTO stages.

presence of oxygen below 300 °C and reduced the energy for chemical bond breakage and accelerated the conversion of kerogen into bitumen and oil/gas [6]. However, after low-temperature pretreatment the total mass loss of organic matter in the combustion process also increased. This may be due to that at low temperature oil shale reacts with oxygen, which makes the fixed carbon and some inorganic minerals decompose in advance.

The kinetics of oil shale in the combustion process, which combines thermal and oxidation effects in the presence of oxygen, is in general extremely complicated. It is well known that solid residues undergo several reactions during the low-temperature preheating treatment.

Figure 4 presents the plot of $\ln[-\ln(1-x)/T^2]$ vs $1/T$ for three stages of pyrolysis of HD oil shale samples at temperatures ranging from 250 to 550 °C and a heating rate of 10 °C min⁻¹. The symbols represent the

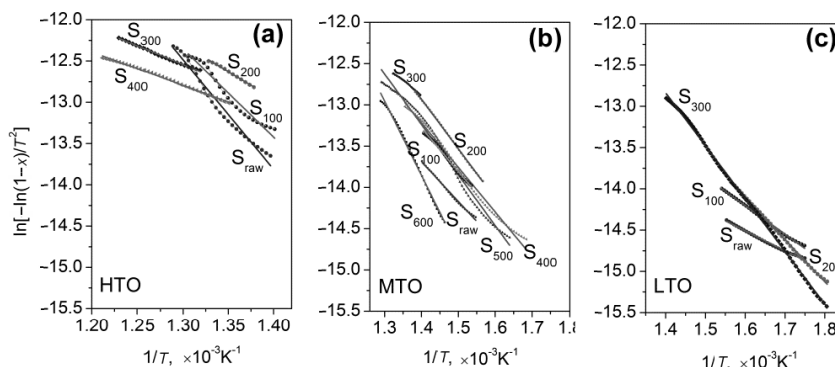


Fig. 4. C-R plots for (a) HTO, (b) MTO and (c) LTO of HD oil shale samples at a heating rate of 10 °C min⁻¹.

scattering experimental data of a sample and the straight lines represent the corresponding fitted line of the data. From the slope and intercept of the line, E and A can be calculated, the results are given in Table 4. It can be seen from the table that the calculated A and E are in excellent correlation with the R^2 coefficient ranging from 0.9669 to 0.9992, which supports the assumption about the first-order kinetics mentioned above.

Figure 5 demonstrates that the E of S_{raw} , S_{100} , S_{200} and S_{300} varies. In the LTO stage, the activation energies of S_{raw} , S_{100} , S_{200} and S_{300} slightly rise, but in HTO are remarkably decreased. The activation energy of each individual sample in each reaction stage can be notionally attributed to different reaction mechanisms; nonetheless, it does not give any indication of the overall reactivity of oil shale and its solid residues. Also, it is difficult to determine whether there is a clear relationship between the activation energies of these samples at a heating rate of $10\text{ }^\circ\text{C min}^{-1}$. Therefore, the concept of weighted

Table 4. Kinetic parameters (E and A) of HD oil shale samples calculated from the C-R method at a heating rate of $10\text{ }^\circ\text{C min}^{-1}$

Sample label	LTO			MTO			HTO			$E_{\text{syn}}, \text{kJ}\cdot\text{mol}^{-1}$
	$E, \text{kJ}\cdot\text{mol}^{-1}$	A, min^{-1}	R^2	$E, \text{kJ}\cdot\text{mol}^{-1}$	A, min^{-1}	R^2	$E, \text{kJ}\cdot\text{mol}^{-1}$	A, min^{-1}	R^2	
S_{raw}	20.04	0.57	0.9938	40.04	46.31	0.9956	110.27	$1.54\text{E} + 7$	0.9764	78.48
S_{100}	28.78	6.77	0.9976	43.82	217.75	0.9955	88.89	5013.47	0.9669	60.66
S_{200}	42.67	63.17	0.9992	49.90	1771.481	0.9997	54.38	2.33	0.9962	48.67
S_{300}	53.25	386.54	0.9992	29.71	89.39	0.9943	37.84	11.40	0.9963	47.93
S_{400}				44.93	189.78	0.9922	33.55	21.27	0.9973	41.63
S_{500}				47.94	345.78	0.9859				47.94
S_{600}				66.44	580.33	0.9952				66.44

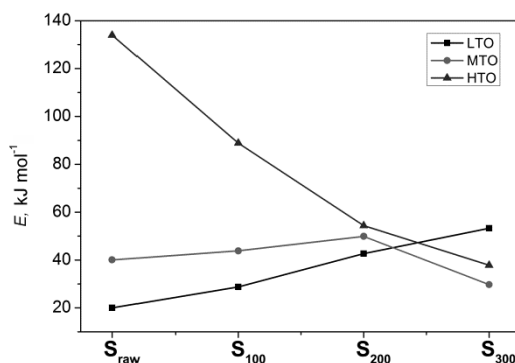


Fig. 5. The activation energies of S_{raw} , S_{100} , S_{200} and S_{300} in LTO, MTO and HTO stages of pyrolysis at a heating rate of $10\text{ }^\circ\text{C min}^{-1}$.

mean activation energy, E_{wm} , is introduced to determine the overall activation energy of the samples [13, 34]:

$$E_{wm} = F_1E_1 + F_2E_2 + F_3E_3 + \dots + F_nE_n, \quad (8)$$

where F_1, F_2, \dots , and F_n are the mass fractions of the sample mass loss during each stage of the Arrhenius linearity, and E_1, E_2, \dots , and E_n are the activation energies of individual samples obtained for each stage.

At a heating rate of $10 \text{ }^\circ\text{C min}^{-1}$, the activation energy (Table 4) decreases from $78.48 \text{ kJ mol}^{-1}$ for S_{raw} to $47.93 \text{ kJ mol}^{-1}$ for S_{300} . Furthermore, it can be seen that the activation energy of S_{100} decreases by 23% compared with that of S_{raw} , but there is almost no change in case of S_{300} and S_{400} . The activation energies of S_{500} and S_{600} increase but are lower than that of S_{raw} .

3.3.2. Effect of heating rate on the kinetics of raw Huadian oil shale and solid residues

TG and DTG curves for the thermal degradation of S_{300} and S_{500} at different heating rates are shown in Figure 6. In this work, increasing the heating rate from 5 to $40 \text{ }^\circ\text{C min}^{-1}$, the characteristic temperatures were shifted to higher values. This is because the heat transfer is not as effective and efficient as it was at lower heating rates [35, 36]. Similarly, with increasing heating rate, the maximum mass loss rates were also shifted to higher temperatures as a consequence of the increasing inertia effect of the devolatilization process [37]. It is also apparent that the extent of diffusion control increases at high heating rates because the products are generated faster than they can diffuse out of the pores, consequently second-order reactions will occur.

From Figure 7 it can be clearly seen that the weighted mean activation energy of samples was greatly affected by heating rate. The activation energy increased with the heating rate changing from 5 to $40 \text{ }^\circ\text{C min}^{-1}$. This may be attributed to the diffusion-limited process controlled by heat, as well as to the temperature difference between the surface and inside of the

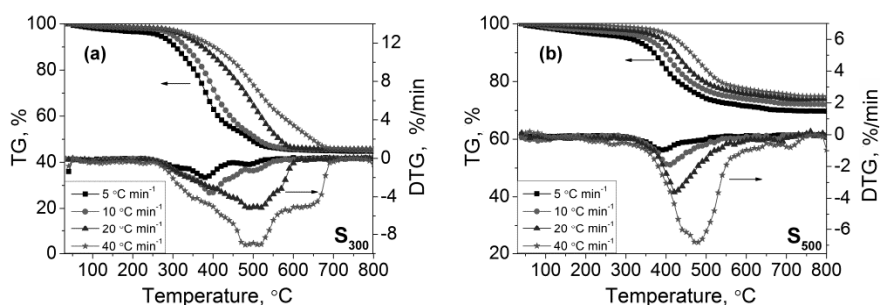


Fig. 6. TG and DTG curves of (a) S_{300} and (b) S_{500} at different heating rates.

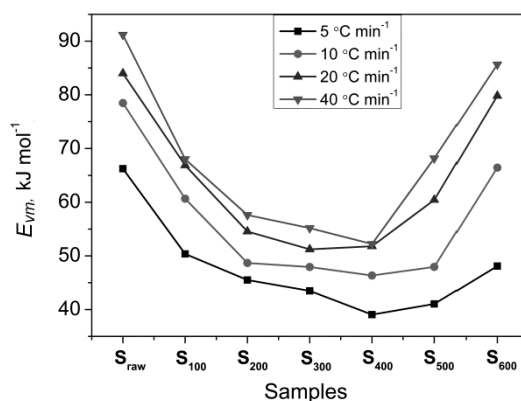


Fig. 7. The weighted mean activation energy of samples at different heating rates.

sample at a higher heating rate [36, 38]. It is obvious that the activation energies of S₁₀₀, S₂₀₀ and S₃₀₀ were reduced at each heating rate. At a heating rate of 5, 10, 20, and 40 °C min⁻¹, the activation energy of S₁₀₀ decreased by 24.98%, 22.7%, 20.39% and 25.40%, respectively, relative to that of S_{raw}.

3.4. Analysis of kinetic characteristics by the FWO method

Applying Equation (7) to the TG data obtained at varying heating rates, plots of $\log \beta$ vs $1/T$ for S_{raw}, S₃₀₀ and S₅₀₀ were constructed (Fig. 8). The activation energies determined from the slope of $\log \beta$ vs. $1/T$ from 10% or 30% to 80% conversion for degradation of organic matter are listed in Table 5. It was found that the activation energies greatly changed, revealing that this degradation is a dominant multi-step kinetic process. The mean activation energy values were 111.76, 98.77, 56.71, 55.40, 90.25, 112.26 and 120.43 kJ mol⁻¹, from S_{raw} to S₆₀₀, respectively. A comparable trend in

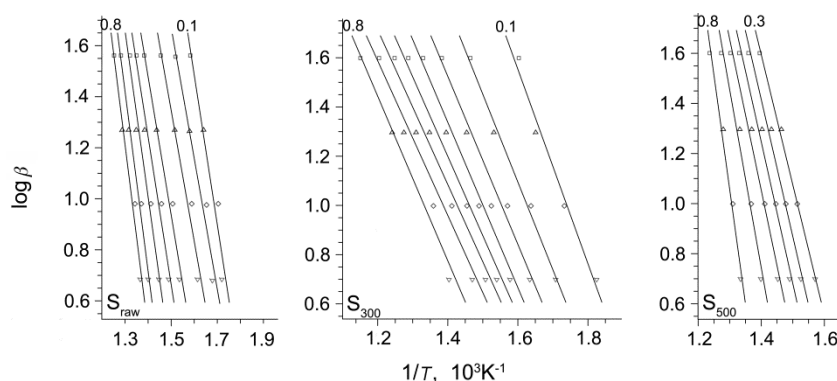


Fig. 8. Plots for the thermal degradation of S_{raw}, S₃₀₀ and S₅₀₀ from FWO.

Table 5. Kinetic parameters (*E* and *A*) of raw HD oil shale and solid residues calculated from the FWO method

Sample label	Conversion degree, %	10	20	30	40	50	60	70	80	Avg
S_{raw}	<i>E</i> , kJ mol ⁻¹	127.35	106.55	93.05	98.85	106.98	113.86	117.95	129.5	111.76
	log(<i>A</i>), s ⁻¹	18.66	6.47	4.83	5.05	5.57	6.00	6.16	6.88	
S_{100}	<i>E</i> , kJ mol ⁻¹	180.11	110.51	105	125.08	99.63	73.14	53.82	42.87	98.77
	log(<i>A</i>), s ⁻¹	13.08	6.06	5.33	6.67	4.58	2.53	1.11	0.35	
S_{200}	<i>E</i> , kJ mol ⁻¹	67.1	61.55	58.77	58.13	55.79	52.67	50.37	49.29	56.71
	log(<i>A</i>), s ⁻¹	2.80	2.18	1.87	1.78	1.57	1.32	1.13	1.04	
S_{300}	<i>E</i> , kJ mol ⁻¹	67.04	59.31	56.04	54.77	52.1	50.31	50.07	53.53	55.40
	log(<i>A</i>), s ⁻¹	2.78	1.95	1.60	1.46	1.24	1.10	1.07	1.29	
S_{400}	<i>E</i> , kJ mol ⁻¹		73.07	73.15	71.73	71.26	76.07	100.37	166.09	90.25
	log(<i>A</i>), s ⁻¹		3.17	3.10	2.95	2.88	3.23	4.92	9.31	
S_{500}	<i>E</i> , kJ mol ⁻¹			89.47	94.26	97.74	104.5	124.64	162.93	112.26
	log(<i>A</i>), s ⁻¹			4.29	4.63	4.87	5.31	6.66	9.10	
S_{600}	<i>E</i> , kJ mol ⁻¹			74.32	99.89	116.88	135.55	135.35	160.56	120.43
	log(<i>A</i>), s ⁻¹			2.83	4.80	6.04	7.32	9.00	13.73	

Note: Avg – average

variation from S_{raw} to S_{600} was also found in the C-R method, but the activation energies calculated by using the latter method were lower than those from the FWO method.

3.5. Evaluation of partially oxidized oil shale

The pyrolysis of kerogen is quite a complex process; it involves reactions of various free radicals, which are greatly affected by reaction conditions [5, 39, 40]. After low-temperature (below 300 °C) partial oxidation treatment under atmospheric conditions, oil shale is supposed to be activated and thus more active sites enhance subsequent reactions [5]. Therefore, preheating treatment possibly accelerates the pyrolysis of organic matter in oil shale via reaction pathways of different free radicals. Moreover, the oxidation of carbonaceous materials occurs on surface carbon sites that are capable of dissociatively chemisorbing oxygen [41]. These sites are primarily associated with the edge or defects on the surface. The amount of these reactive sites is known to be strongly dependent on parameters such as surface area [42], and it is reasonable that the release of some water and slight volatile species, which are produced by the mild oxidation reaction of carbonaceous fuels, increases the surface area of sample. Hence, samples having a high surface area after preheating treatment are more reactive. Moreover, the increase of opening pore structures provides a heat transmission channel. As reported by Lázaro et al. [43], high temperature or long time is usually required for a high activation energy reaction. It is logical that the decomposition of organic matter mainly takes place from 300 to 550 °C [44, 45]. Furthermore, there is no marked loss in oil yield after preheating treatment below 300 °C [5, 6]. Therefore, it is noted that the

decomposition reaction above 300 °C could be enhanced effectively through preheating the samples, which is advantageous for the organic matter converting into shale oil/gas, especially in in situ extraction.

Based on TG the activation energies of S_{500} and S_{600} increase at each heating rate but are lower than that of S_{raw} . This gradual increase in activation energy at high preheating temperatures may be associated with the high degree of carbonization. Oil shale pyrolyzed at higher temperatures, differently from that pyrolyzed at lower temperatures, tends to have a lower content of volatiles, hydrogen and oxygen, and a lower degree of disorder [46, 47]. Moreover, much more energy is required for the decomposition of inorganic mineral, which makes oil shale pyrolysis highly energy-consuming. Pyrite, for instance, is oxidized between 450 and 550 °C, its activation energy on the phase transformation is 136.77 kJ mol⁻¹; furthermore, the activation energy of the mixture of coal and pyrite is higher than that of raw coal [48].

4. Conclusions

In this research, TG data were used to estimate the kinetic parameters of both raw Huadian oil shale and its solid residues after preheating treatment at different temperatures. The results showed that:

- Pyrolysis of raw oil shale takes place in several stages at temperatures ranging from 250 to 550 °C, known as low-temperature, moderate-temperature and high-temperature oxidation. This paper analyzed the kinetics of oxidized oil shale between 250 to 550 °C by using the Coats-Redfern and Flynn-Wall-Ozawa methods. The variation of activation energy from S_{raw} to S_{600} in the two methods showed an almost similar trend.
- The burning of oil shale and its solid residues is a complicated multi-step kinetic process. As the preheating temperature increased, the thermal reactions of oil shale took place. The activation energies of S_{100} , S_{200} and S_{300} were reduced contrary to that of S_{raw} . At a preheating temperature above 400 °C, the activation energy increased with increasing pretreatment temperature, and more kerogen was driven out during partial oxidation at higher preheating temperatures.
- In the Coats-Redfern method, the activation energies of oil shale samples increased with increasing heating rate. This is due to the differences in the rate of heat transfer and product diffusion to sample, which occurred with variation in heating rate.

However, it should be noted that this paper studied only the activation energy of Huadian oil shale after partial oxidation; the applicability of conclusions to practice yet remains to be elucidated in further research.

Acknowledgment

This work was supported by the National Cooperative Innovation Project on Chinese Potential Oil and Gas Resources (Grant No. OSR-06) and the Graduate Innovation Fund of Jilin University, China (Grant No. 2014064).

REFERENCES

1. Pan, Y., Zhang, X. M., Liu, S. H., Yang, S. C., Ren, N. A Review on technologies for oil shale surface retort. *J. Chem. Soc. Pak.*, 2012, **34**(6), 1331–1338.
2. Liu, D. X., Wang, H. Y., Zheng, D. W., Fang, C. H., Ge, Z. X. World progress of oil shale in-situ exploitation methods. *Natural Gas Industry*, 2009, **29**, 128–132 (in Chinese).
3. Jiang, X. M., Han, X. X., Cui, Z. G. Progress and recent utilization trends in combustion of Chinese oil shale. *Prog. Energ. Combust.*, 2007, **33**(6), 552–579.
4. Niu, M. T., Wang, S., Han, X. X., Jiang, X. M. Yield and characteristics of shale oil from the retorting of oil shale and fine oil-shale ash mixtures. *Appl. Energ.*, 2013, **111**, 234–239.
5. Guo, H. F., Peng, S. Y., Lin, J. D., Chang, J., Lei, S., Fan, T. B., Liu, Y. Y. Retorting oil shale by a self-heating route. *Energ. Fuel*, 2013, **27**, 2445–2451.
6. Sun, Y. H., Bai, F. T., Liu, B. C., Liu, Y. M., Guo, M. Y., Guo, W., Wang, Q. W., Lü, X. S., Yang, F., Yang, Y. Characterization of the oil shale products derived via topochemical reaction method. *Fuel*, 2014, **115**, 338–346.
7. Martins, M. F., Salvador, S., Thovert, J.-F., Debenest, G. Co-current combustion of oil shale – Part 1: Characterization of the solid and gaseous products. *Fuel*, 2010, **89**(1), 144–151.
8. Bhargava, S., Awaja, F., Subasinghe, N. D. Characterisation of some Australian oil shale using thermal, X-ray and IR techniques. *Fuel*, 2005, **84**(6), 707–715.
9. Jaber, J. O., Probert, S. D. Non-isothermal thermogravimetry and decomposition kinetics of two Jordanian oil shales under different processing conditions. *Fuel Process. Technol.*, 2000, **63**(1), 57–70.
10. Rajeshwar, K., Nottenburg, R., Dubow, J. Thermophysical properties of oil shales. *J. Mater. Sci.*, 1979, **14**(9), 2025–2052.
11. Kök, M. V. Heating rate effect on the DSC kinetics of oil shales. *J. Therm. Anal. Calorim.*, 2007, **90**(3), 817–821.
12. Kök, M. V. Effect of clay on crude oil combustion by thermal analysis techniques. *J. Therm. Anal. Calorim.*, 2006, **84**(2), 361–366.
13. Kök, M. V., Pokol, G., Keskin, C., Madarász, J., Bagci, S. Light crude oil combustion in the presence of limestone matrix. *J. Therm. Anal. Calorim.*, 2004, **75**(3), 781–786.
14. Kök, M. V., Pamir, R. Pyrolysis kinetics of oil shales determined by DSC and TG/DTG. *Oil Shale*, 2003, **20**(1), 57–68.
15. Kök, M. V., Pokol, G., Keskin, C., Madarász, J., Bagci, S. Combustion characteristics of lignite and oil shale samples by thermal analysis techniques. *J. Therm. Anal. Calorim.*, 2004, **76**(1), 247–254.

16. Kok, M. V., Senguler, I., Hufnagel, H., Sonel, N. Thermal and geochemical investigation of Seyitomer oil shale. *Thermochim. Acta*, 2001, **371**(1–2), 111–119.
17. Kök, M. V., Iscan, A. G. Oil shale kinetics by differential methods. *J. Therm. Anal. Calorim.*, 2007, **88**(3), 657–661.
18. Jiang, X. M., Han, X. X., Cui, Z. G. Mechanism and mathematical model of Huadian oil shale pyrolysis. *J. Therm. Anal. Calorim.*, 2006, **86**(2), 457–462.
19. Yan, J. W., Jiang, X. M., Han, X. X. Study on the characteristics of the oil shale and shale char mixture pyrolysis. *Energ. Fuel*, 2009, **23**, 5792–5797.
20. Khan, M. R. Influence of weathering and low-temperature preoxidation on oil shale and coal devolatilization. *Energ. Fuel*, 1987, **1**(4), 366–376.
21. Coats, A. W., Redfern, J. P. Kinetic parameters from thermogravimetric data. *Nature*, 1964, **201**, 68–69.
22. Flynn, J. H., Wall, L. A. A quick, direct method for the determination of activation energy from thermogravimetric data. *J. Polym. Sci. Part B. Pol. Lett.*, 1966, **4**(5), 323–328.
23. Ozawa, T. A new method of analyzing thermogravimetric data. *Bull. Chem. Soc. Jpn.*, 1965, **38**, 1881–1886.
24. Doyle, C. Kinetic analysis of thermogravimetric data. *J. Appl. Polym. Sci.*, 1961, **5**(15), 285–292.
25. Opfermann, J., Kaisersberger, E. An advantageous variant of the Ozawa-Flynn-Wall analysis. *Thermochim. Acta*, 1992, **203**, 167–175.
26. López-Fonseca, R., Landa, I., Gutiérrez-Ortiz, M. A., González-Velasco, J. R. Non-isothermal analysis of the kinetics of the combustion of carbonaceous materials. *J. Therm. Anal. Calorim.*, 2005, **80**(1), 65–69.
27. Tonbul, Y. Pyrolysis of pistachio shell as a biomass. *J. Therm. Anal. Calorim.*, 2008, **91**(2), 641–647.
28. Zhang, N.X. *The research methods for clay minerals*. First ed.: Science Press, Beijing, 1990.
29. Altun, N. E., Hwang, J.-Y., Hicyilmaz, C. Enhancement of flotation performance of oil shale cleaning by ultrasonic treatment. *Int. J. Miner. Process.*, 2009, **91**(1–2), 1–13.
30. Ruan, J. S., Bai, W. Analysis and application of infra-red spectra for kerogen. *Exp. Petro. Geol.*, 1988, **10**, 80–86 (in Chinese).
31. Adams, M. J., Awaja, F., Bhargava, S., Grocott, S., Romeo, M. Prediction of oil yield from oil shale minerals using diffuse reflectance infrared Fourier transform spectroscopy. *Fuel*, 2005, **84**(14–15), 1986–1991.
32. Ganz, H. H., Kalkreuth, W. IR classification of kerogen type, thermal maturation, hydrocarbon potential and lithological characteristics. *J. Southe. Asian Earth*, 1991, **5**(1–4), 19–28.
33. Grice, K., Schouten, S., Blokker, P., Derenne, S., Largeau, C., Nissenbaum, A., Sinninghe Damste, J. S. Structural and isotopic analysis of kerogens in sediments rich in free sulfurised *Botryococcus braunii* biomarkers. *Org. Geochem.*, 2003, **34**(3), 471–482.
34. Cumming, J. W., McLaughlin, J. The thermogravimetric behaviour of coal. *Thermochim. Acta*, 1982, **57**(3), 253–272.
35. Idris, S. S., Abd Rahman, N., Ismail, K., Alias, A. B., Abd Rashid, Z., Aris, M. J. Investigation on thermochemical behaviour of low rank Malaysian coal, oil palm biomass and their blends during pyrolysis via thermogravimetric analysis (TGA). *Bioresource Technol.*, 2010, **101**(12), 4584–4592.

36. Williams, P. T., Ahmad, N. Investigation of oil-shale pyrolysis processing conditions using thermogravimetric analysis. *Appl. Energ.*, 2000, **66**(2), 113–133.
37. Lapuerta, M., Hernández, J. J., Rodríguez, J. Kinetics of devolatilisation of forestry wastes from thermogravimetric analysis. *Biomass Bioenerg.*, 2004, **27**(4), 385–391.
38. Rajeshwar, K. Thermal analysis of coals, oil shales and oil sands. *Thermochem. Acta*, 1983, **63**(1), 97–112.
39. Wahyudiono, Shiraishi, T., Sasaki, M., Goto, M. Non-catalytic liquefaction of bitumen with hydrothermal/solvothermal process. *J. Supercrit. Fluid.*, 2011, **60**, 127–136.
40. Pan, C. C., Geng, A. S., Zhong, N. N., Liu, J. Z., Yu, L. P. Kerogen pyrolysis in the presence and absence of water and minerals 1. Gas components. *Energ. Fuel.*, 2008, **22**, 416–427.
41. Stanmore, B. R., Brillhac, J. F., Gilot, P. The oxidation of soot: a review of experiments, mechanisms and models. *Carbon*, 2001, **39**(15), 2247–2268.
42. Su, D. S., Müller, J.-O., Jentoft, R. E., Rothe, D., Jacob, E., Schlögl, R. Fullerene-like soot from EuroIV diesel engine: consequences for catalytic automotive pollution control. *Top. Catal.*, 2004, **30/31**(1–4), 241–245.
43. Lázaro, M. J., Moliner, R., Suelves, I. Non-isothermal versus isothermal technique to evaluate kinetic parameters of coal pyrolysis. *J. Anal. Appl. Pyrol.*, 1998, **47**(2), 111–125.
44. Qian, J. L., Yin, L. *Oil Shale – Supplementary Energy of Petroleum*. China Petrochemical Press, Beijing, 2011 (in Chinese).
45. Hubbard, A. B., Robinson, W. E., Savage, J. W. *A thermal decomposition study of Colorado oil shale*. Bureau of Mines, Washington, DC, 1950.
46. Goldfarb, J. L., D'Amico, A., Culin, C., Suuberg, E. M., Külaots, I. Oxidation kinetics of oil shale semicokes: reactivity as a function of pyrolysis temperature and shale origin. *Energ. Fuel.*, 2013, **27**(2), 666–672.
47. Külaots, I., Goldfarb, J. L., Suuberg, E. M. Characterization of Chinese, American and Estonian oil shale semicokes and their sorptive potential. *Fuel*, 2010, **89**(11), 3300–3306.
48. Borah, D., Barua, M., Baruah, M. K. Dependence of pyrite concentration on kinetics and thermodynamics of coal pyrolysis in non-isothermal systems. *Fuel Process. Technol.*, 2005, **86**(9), 977–993.

Presented by J. Kann and M. V. Kök

Received November 27, 2013